The LNE-LNHB water calorimeter for primary measurement of absorbed dose at low depth in water: application to medium-energy x-rays

Benjamin Rapp, Nicolas Perichon, Marc Denozière, Josiane Daures, Aimé Ostrowsky, jean-marc bordy

LNE-LNHB water calorimeter for primary measurement of absorbed dose at low depth in water. Application to medium energy X-rays.

B. Rapp, N. Perichon, M. Denoziere, J. Daures, A. Ostrowsky and J-M. Bordy

CEA, LIST, Laboratoire National Henri Becquerel (LNE-LNHB)
F-91191 Gif-sur-Yvette, France.

E-mail: benjamin.rapp@cea.fr

Abstract.

Water calorimeters are used to establish absorbed dose standards in several national metrology laboratories involved in ionizing radiation dosimetry. These calorimeters have been first used in high energy photons of ^{60}Co or accelerators beams, where the depth of measurement in water is large (5 or 10 cm). The LNE-LNHB laboratory has developed a specific calorimeter which makes measurements at low depth in water (down to 0.5 cm) easier, in order to fulfill the reference conditions required by the international dosimetry protocols for medium energy X-rays. This new calorimeter was first used to measure the absorbed dose rate in water at a depth of 2 cm for 6 medium energy X-ray reference beams with a tube potential from 80 kV to 300 kV. The relative combined standard uncertainty obtained on the absorbed dose rate to water is lower than 0.8 %. An overview of the design of the calorimeter is given, followed by a detailed description of the calculation of the correction factors and the calorimetric measurements.

Keywords: Water Calorimeter, Absorbed Dose, Medium Energy X-Rays, Primary Dosimetry

1. Introduction

The dosimetry protocols of IAEA (International Atomic Energy Agency) TRS–277 [1], AAPM (The American Association of Physicists in Medicine) TG–61 [2], IPEMB [3] and NCS–10 [4] for medium-energy X-ray beams are widely used by medical physicists in hospitals to calculate the absorbed dose to water from air-kerma calibrated ionization chamber. When absorbed dose to water references will be available, the protocol of IAEA TRS-398 [5] will be used by medical physicists for medium energy X-rays. The protocols TG–61, IPEMB and NCS–10 recommends a 2 cm reference depth in water, whereas the protocol TRS–277 gives a depth of 5 cm. The protocol TRS–398, which will be more used in the future, recommends a reference depth in water of 2 g.cm^{-2}. All these protocols recommends a 10×10 cm^2 field size defined at a distance between 50 and 100 cm from the source. J. Seuntjens (University of Gent, Belgium) [6], and some primary standard dosimetry laboratories like VSL (Van Swinden Laboratorium, Netherlands) [7] and PTB (Physikalisch-Technische Bundesanstalt, Germany) [8, 9] already did primary measurements with a water calorimeter for medium-energy X-rays, but with reference conditions often quite different from the ones given by dosimetry protocols. For example at VSL, a measurement depth in water of 3.6 g.cm^{-2} was used, at a distance of 61.5 cm with a circular radiation field of ∅8 cm. The main reason for this situation is that water calorimeters were first designed for high-energy photons in ^{60}Co or accelerator beams, where the depth of measurement in water is large (5 or 10 g.cm^{-2}). This is why we have developed a specific water calorimeter to do measurements at low depth in water (down to 0.5 cm from the surface of the water phantom), in order to fulfill the reference conditions required by international dosimetry protocols for medium energy X-rays. Thus a more direct comparison between primary measurements of absorbed dose to water and the application of protocols based on air-kerma is possible. This comparison, based on the calorimetric measurements reported here, is discussed in a second paper [10].

The newly built calorimeter was used to measure the absorbed dose rate to water for 6 reference beams of medium-energy X-rays between 80 kV and 300 kV [11]. The choice of these reference beams was done on the basis of the performances of the X-ray generator used for measurements, among reference beams already characterized in air-kerma at LNE-LNHB [12] and delivering an absorbed dose rate to water large enough (>0.3 Gy.min^{-1}) to do water calorimetry measurements. The X-ray generator used for measurements is a SEIFERT 320 kV ISOVOLT HS [13] with a COMET MXR-350/26 [14] X-ray tube. The stability of the generator was tested for each of the reference beams. Some periodical measurements were done over several days, with an NE 2571 ionization chamber. The results showed a stability better than 0.1% over a week. Then it was chosen not to monitor the beam continuously, but instead to check the stability once a week before each series of calorimetric measurements.

The characteristics of these beams like tube potential, additional filtration, half-value layer (HVL), and mean energy (calculated from simulated photon fluence spectra)

are given in the Table 1.

Table 1. Characteristics of the reference beams of medium-energy X-rays chosen for water calorimetry measurements.

X-ray beam ref.	Tube potential (kV)	Additional filtration	HVL	$E_{mean,\phi}$ (keV)
RQR6	80	2.50 Al mm	3.01 Al mm	44
RQR9	120	2.50 Al mm	5.00 Al mm	56
RQR10	150	2.50 Al mm	6.57 Al mm	63
CCRI180	180	4.06 Al + 0.51 Cu mm	1.00 Cu mm	85
CCRI250	250	4.02 Al + 1.72 Cu mm	2.50 Cu mm	120
ISOH300	300	4.00 Al + 2.50 Cu mm	3.40 Cu mm	141

2. The LNE-LNHB water calorimeter design

2.1. General overview

The new water calorimeter of LNE-LNHB was built taking into consideration the experience of other metrology laboratories [15] and our own experience in water calorimetry [16, 17] for measurements in high-energy photon beams. Thus, the calorimeter was designed to operate at 4 °C, the temperature of the maximum density of water, to minimize convective currents inside the water volume used for measurements. The inner part of the water calorimeter consists of a radiotherapy water phantom of $30 \times 30 \times 35$ cm^3 built with PMMA of 15 mm thickness, and filled with demineralized water. Some pictures of the calorimeter can be seen in Figure 1.

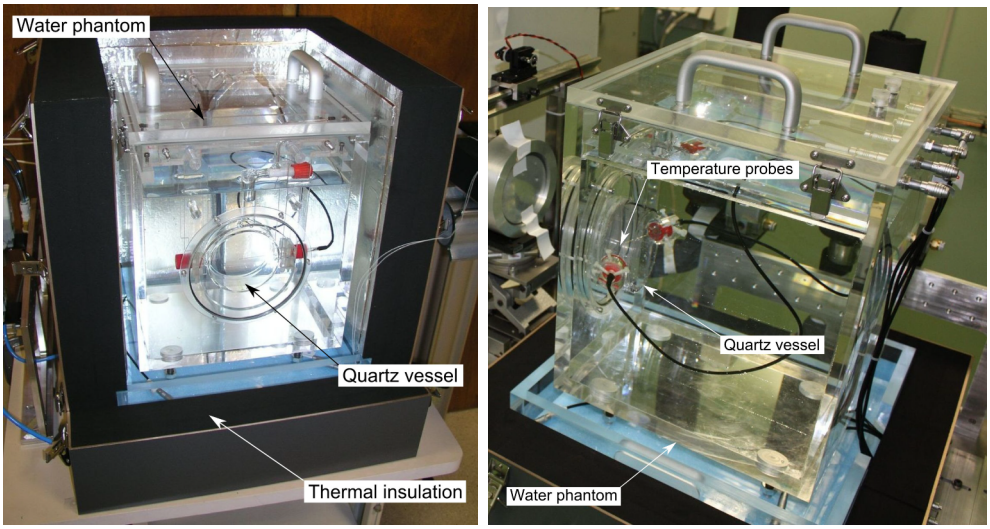

Figure 1. Front view (on left) and side view (on right) of the water calorimeter.

The temperature rise is measured by two thermistor probes, placed inside a cylindrical quartz vessel filled with high-purity water. This quartz vessel can be inserted

in the front face of the water phantom (for measurements at low depth in water) or placed at any depth in the water phantom. In both cases, the calorimeter is suitable for use with horizontal beams only. To insert the quartz vessel in the front face of the water phantom, the vessel is sealed in a PMMA ring with a silicon joint. This ring is fixed with screws to the front face of the water phantom, and sealed with a rubber joint around it. A schematic horizontal section of the calorimeter centered on the quartz vessel is shown in Figure 2.

The temperature of the water phantom is regulated (at 4 °C) by a cold air circulation inside a 20 mm gap between the phantom and the thermal enclosure. The thermal enclosure, that is needed to insulate against ambient temperature fluctuations, consists of a thick layer (80 mm) of extruded polystyrene inside a PVC box of 4 mm thickness. There is a window of 12 × 12 cm^2 area in the thermal enclosure with a reduced thickness of materials on the beam axis (24 mm of extruded polystyrene slab and a Mylar sheet of 0.1 mm).

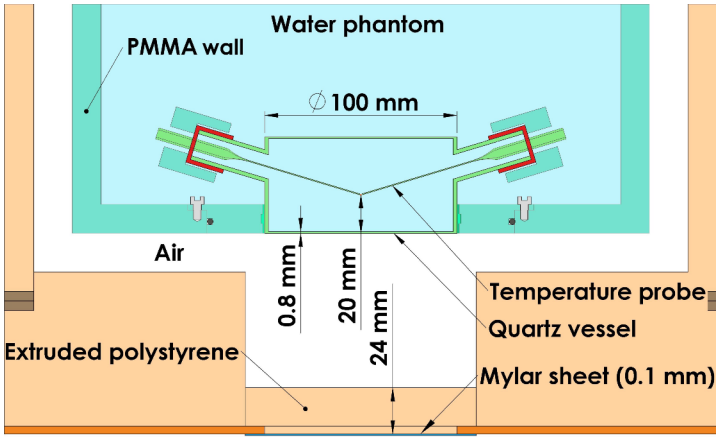

Figure 2. Schematic horizontal section of the water calorimeter.

2.2. Air regulation system of the new calorimeter

The thermal regulation of water calorimeters can be done with a circulation of water or air. Water circulation is generally preferred because the thermal transfers between the water phantom and the circulating water are more efficient than with air, and the thermal regulation of water is easier and more direct. But calorimeters with a system of water regulation are heavy and difficult to carry to different places. No water circulation must be present in the beam path because of the absorption and scattering induced. The absence of a cooling medium, in front of the measurement point, results in a thermal leakage demanding a large thermal insulation in the beam path.

Until now, air-regulated calorimeters have a large air gap around the water phantom. This large air gap between thermal enclosure and water phantom, is maintained at 4 °C by circulating in a secondary water-to-air heat exchanger. Some

rotating fans are used inside the thermal enclosure to force air circulation and then obtain a temperature as homogeneous as possible.

In our new calorimeter, the option of air regulation was chosen. But instead of having a finite volume of cold air inside the thermal enclosure and trying to regulate its temperature by using rotating fans and water-to-air heat exchangers, we decided to inject a strong flow of cold air at constant temperature to the calorimeter and let it escape naturally by some openings in the thermal enclosure. This allows a more compact and transportable instrument.

A strong flow of cold air is generated by a commercial vortex tube [18] fed with compressed air and connected to a pressure regulator (see principle diagram of the system in Figure 3). The compressed air is supplied by an industrial distribution network, at a pressure of 7 bar and at ambient temperature. The regulator is part of a PID control loop, programmed with LabView programming environment, in which the process variable is the temperature measured inside the calorimeter thermal enclosure by a thermistor. Two of these systems are used to inject cold air underneath the water phantom, and inside the entrance window of the calorimeter. With this system the temperature of air around the water phantom is maintained in a stationary state around 4 °C. The temperature measurements, made with small thermistors in different locations inside the thermal enclosure, showed the existence of a vertical temperature gradient. However, by adjusting regulation parameters, a stable temperature close to 4 °C was obtained at the surface of the quartz vessel, with a stability of ±0.01 °C over a long period of time (2 days). Inside the quartz vessel, at a depth of 2 cm, the temperature measurement showed a maximum drift of 20 μK.min^{-1} on the same period of time. During our previous studies with water calorimeter in high-energy photon beams, we observed that the influence of a thermal drift lower than 50 μK.min^{-1} on measured temperature rise, is negligible. For comparison, the measured average temperature rise, ranges from $\sim$ 280 to $\sim$ 500μK, following the X-ray beam.

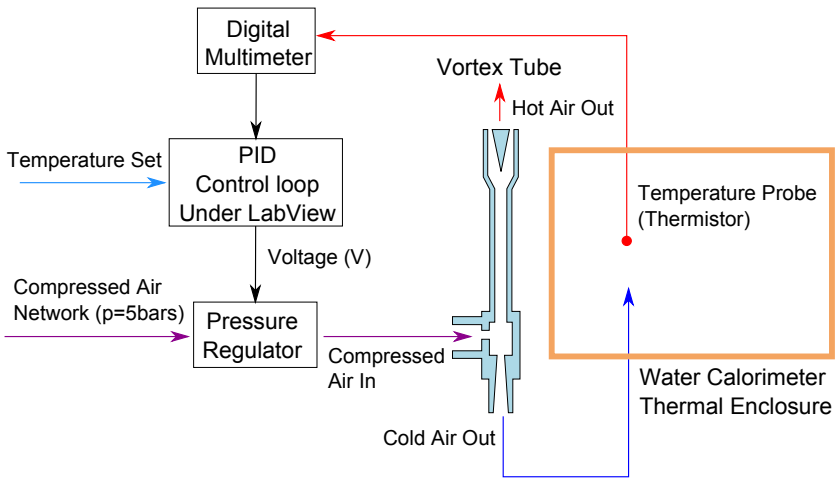

Figure 3. Principle diagram of air regulation system.

2.3. Quartz vessel

Two probes are placed inside a quartz vessel to measure the temperature. The quartz vessel is of cylindrical shape with a diameter of 10 cm and a thickness of 5 cm. Its front and back parallel faces are made of quartz sheets of 0.8 mm of thickness. The quartz vessel is filled with high-purity water saturated with N_2 gas, and pre-irradiated at several hundreds of grays, in order to control the heat defect of water (see Section 3.4). Quartz was chosen to avoid contamination of high-purity water inside the vessel.

In order to do measurements at low depth in water (typically 2 cm for medium energy X-rays) the quartz vessel is inserted in the front wall of the water phantom, as explained in section 2.1 (see Figures 1, 2 and 4). With this design, measurements can be done at a depth down to 0.5 cm in water from the surface of the water phantom. The only limitations are: the thickness of the front face of the quartz vessel, and a direct contact to be avoided between the temperature probe and the quartz vessel front face. Until now, in other primary standard dosimetry laboratories, low-depth measurements were achieved by using the free surface of water on the top of water phantom, for vertical beams only (for example, the McGill University water calorimeter developed to operate in electron beams [19, 20]). Our calorimeter design allows to do measurements at low depth in water in horizontal beams, which is generally more common. All the measurements were done at a depth of 20 mm in the quartz vessel, which includes 0.8 mm of quartz (thickness of the front window of the quartz vessel) and 19.2 mm of water. It has been chosen to do measurements not exactly at 2 g.cm^{-2} in water, as required by dosimetry protocols, because the water equivalence of quartz is not well known for kilo-voltage X-rays. To overcome this problem, the measurements made with ionization chambers to calibrate them in absorbed dose to water [10] were done at the same depth, in a special PMMA water phantom with a quartz window of 0.8 mm of thickness.

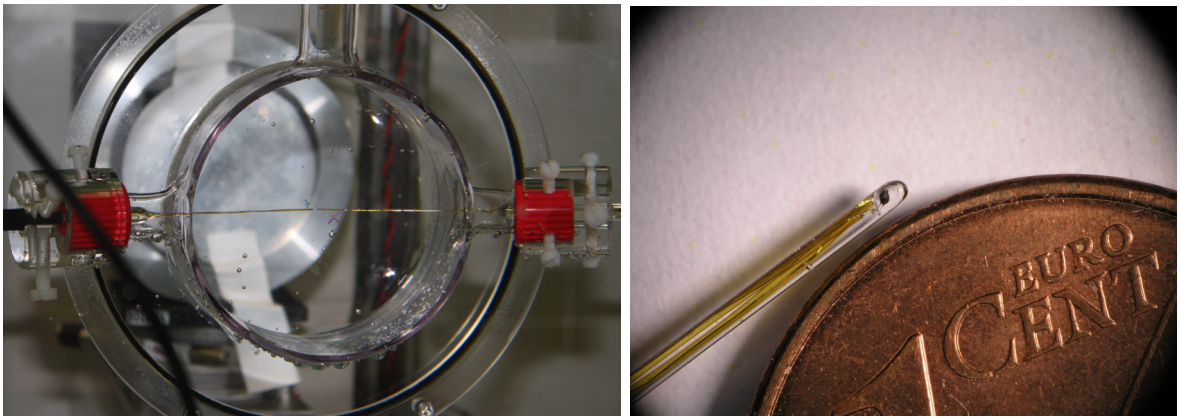

Figure 4. On the left, a picture of the quartz vessel filled with high-purity water saturated with N_2 gas, in which are placed two temperature probes. On the right, a picture of a temperature probe. The thermistor bead is visible at the end of the quartz capillary.

2.4. Temperature probes

A temperature probe (see Figure 4) consists of a sealed quartz capillary of 0.6 mm outer diameter with a negative-temperature-coefficient (NTC) thermistor inside. The NTC thermistor (BR11KA432J reference produced by General Electric [21]) is glass-encapsulated and has a nominal resistance of 4300 Ω at 25 °C (or ∼ 9300 Ω at 4 °C), and a diameter of 0.28 mm. The thermistor is connected to a cable through Pt/Ir wires (⌀0.05 mm) electrically insulated with Kapton tubes [22] (⌀0.18 mm). The capillary is filled with epoxy resin under vacuum to avoid air bubbles.

The resistance of the thermistors of the two temperature probes are measured by two DC Wheatstone bridges built with high-precision resistors of 8000 Ω, connected to a precision voltmeter. The bridges are used near equilibrium without re-balancing after each irradiation; instead the bridge equation is applied to calculate the resistance of the thermistors. Each temperature probe is calibrated with its own bridge and voltmeter, so the parameters of the bridge need not be known accurately. DC Wheatstone bridges have been chosen deliberately instead of AC bridges. The DC bridges can be noisier than the AC ones, but their calibration is easier and more stable. Moreover, no further calibration is needed during the measurement process.

The calibration of the temperatures probes is done by comparison with a Standard Platinum Resistance Thermometer (SPRT), itself calibrated by the French primary metrology laboratory for temperature measurements (LNE-LCM). For calibration, the probes are immersed in water, in a deep calibration bath with a high temperature homogeneity and stability. The temperature of the bath is changed in steps from 1 °C to 8 °C. The thermistor equation is used over this range of temperature for fitting the measured resistance of the thermistor, as function of the bath temperature given by the SPRT:

$$R = R(T_0)e^{\beta(1/T-1/T_0)} \tag{1}$$

With $R(T_0)$ the resistance at temperature T_0 and β the material constant of the thermistor. The final relative uncertainty on the temperature rise measurement resulting from this calibration is estimated to 0.1%. The calibration of the temperature probes is done with the electronics also used for calorimetry measurements. In this way, the Wheatstone bridges and voltmeters used for readout do not need to be calibrated.

2.5. Positioning of temperature probes in water

The positioning of temperature probes inside the quartz vessel can be done only after filling the vessel with ultra-pure water. So only an optical method can be used. For this task a long working-distance microscope objective is placed on the head of a video camera mounted on a motorized micro-metric translation stage. The working distance of this objective (distance between the front end of objective and the surface to observe) is of 34 mm in air, and the depth of field is 14 μm.

A distance measurement is obtained from the translation stage by focusing alternatively on the thermistor bead of the temperature probe and the external surface of the quartz vessel. This measurement has to be corrected for the refraction of light in water and quartz to obtain the real depth of thermistor in quartz vessel. The absolute accuracy of the motorized micro-metric translation stage was measured by the supplier (Newport Corporation), and is lower than 10 μm. The relative standard uncertainty on the distance measurement, with this optical system was estimated at 50 μm. The accuracy has been checked with glass plane plates used as windows in optical systems. These plane plates are made of an optical glass with a well known refraction index. The thickness of the plane plates (10 mm and 20 mm) were measured with the optical system, and were compared with measurements made with a calibrated micrometer. The measurements were compatible taking into consideration the relative standard uncertainty of the optical system. So, with such a device, the depth in the quartz vessel of the thermistor of the temperature probe can be measured with a relative standard uncertainty of 50 μm ($k = 1$).

3. Measurement principle and correction factors

The absorbed dose to water (D_W) is determined from the temperature rise measurement by the following equation :

$$D_W = C_p \Delta T (1-h)^{-1} k_p k_c k_\rho k_d \tag{2}$$

where C_p the specific heat capacity of water at 4 °C, ΔT is the measured temperature rise under irradiation, h is the water chemical heat defect, k_p the radiation field perturbation correction factor, k_c the thermal conduction correction factor, k_ρ the density of water correction factor and k_d the depth in water correction factor.

The specific heat capacity of water at 4 °C has been taken as 4204.8 J.kg^{-1}.K^{-1}. This value is calculated from a polynomial equation given in the *Journal of Physical and Chemical Reference Data* [23]. This polynomial equation is based on a set of experimental data published in 1939 by N.S. Osborne [24]. The relative uncertainty of this set of data is not well documented, but is estimated to be between 0.01 and 0.02% in the *Journal of Physical and Chemical Reference Data*. So, the relative uncertainty on the specific heat capacity of water has been enlarged to 0.1%.

3.1. Temperature rise measurement (ΔT)

The low thermal diffusivity of water allows the measurement of a local temperature rise over a timescale of a few minutes. The choice of the irradiation time is a compromise between a good signal-to-noise ratio and a minimization of thermal transfer effects on the temperature rise measurement. The irradiation scheme is a sequence of 3 irradiations of 4 min, followed by a pause time of 1.5 h to allow the cone of heat produced by irradiation in water to vanish. The determination of the temperature rise (ΔT) is done by an extrapolation to mid-irradiation of the linear fits of the temperature drift before

and after irradiation. An example of temperature rise measurement for the ISOH300 X-ray beam is given in Figure 5.

The data obtained immediately after the irradiation stop are not taken into account because this period is sensitive to the thermal effect caused by the temperature probes (see Section 3.2.2). The value of temperature rise (ΔT) changes with the delay of post-irradiation measurements chosen after the irradiation stop. The thermal conduction correction factor (k_c) varies also with the delay of post-irradiation measurements, because it is calculated by applying the same extrapolation method. For a post-irradiation measurement delay varying from 10 s (or 40 s) to 80 s after the irradiation stop the effect on the absorbed dose, after applying the thermal conduction correction factor, is less than 0.1% for ISOH300 and CCRI250 beams, and larger (0.2–0.4%) for other beams. This effect was included in the calculation of uncertainty of the thermal conduction correction factor.

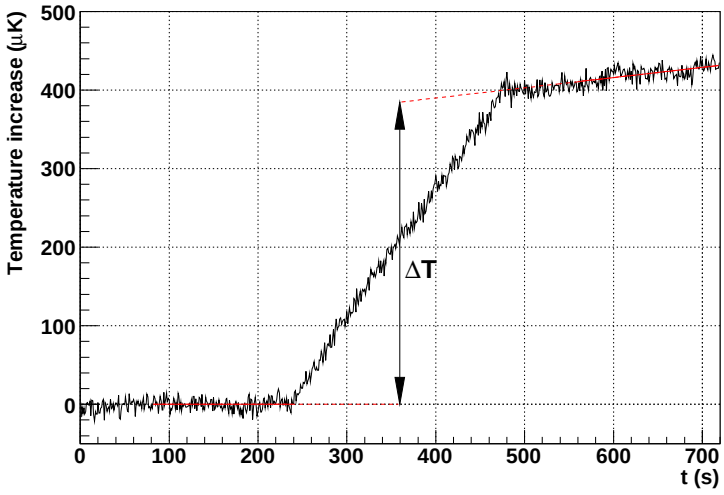

Figure 5. Example of temperature rise measurement for the ISOH300 X-ray beam.

3.2. Thermal conduction correction factor (k_c)

The thermal transfers in water occur by conduction and convection, but natural convective thermal transfers are minimized by operating at 4 °C at the maximum density of water. Then, a correction factor named k_c, taking account of thermal transfers by conduction is applied to the measurements. To evaluate this correction factor a Monte-Carlo simulation of the heat deposition in the water phantom by radiation is combined with the calculation of the heat transfers by conduction in the calorimeter.

3.2.1. Monte-Carlo simulations The MCNPX Monte-Carlo code [25] has been used to obtain the absorbed dose distribution in the water calorimeter. For this, a three-step simulation was done.

The first step consists in a detailed simulation of the X-ray tube. The bremsstrahlung process for the electrons hitting a thin tungsten target (2.5 mm of thickness) in vacuum is simulated, and the photons produced are transported through two beryllium windows (2 mm + 1 mm thickness) before leaving the X-ray tube. This calculation is time consuming because it involves a detailed transport of a large number of photons and electrons. This is why the characteristics of the particles escaping the X-ray tube are recorded in a phase space file that is used in further simulations.

In the second step, the photon fluence spectrum in air at a distance of 18 cm from the X-ray tube is recorded. For this, the previous phase space file is used as input, and particles are transported in air through the primary lead collimator (a hole of ∅55 mm) and additional filtration (Al and/or Cu filters) of the X-ray tube. The number of particles generated in the phase space file is large enough to obtain sufficient statistics in the photon fluence spectrum, but not enough to obtain the desired statistics on the absorbed dose at 2 cm in water and a distance of 50 cm. For this reason, and also to simplify the simulation, the choice was made to model the X-ray beam issued from the tube only using the photon fluence spectrum.

Finally, in the third simulation step the absorbed-dose distribution in the water calorimeter is obtained. The X-ray source is described as a photon point source with the previous calculated photon fluence spectrum. The secondary lead collimator defining a 10×10 cm^2 radiation field is included in the simulation. A simplified geometry of the thermal enclosure and water phantom of the calorimeter is used (see Figure 6). Inside the water phantom the geometry of the quartz vessel is included. The two temperature probes (quartz capillary of ∅0.6 mm filled with epoxy resin and glass-encapsulated thermistor with Pt/Ir wires) are also included. The absorbed dose distribution in water is recorded using the MCNPX mesh tallies. Inside temperature probes, the total energy deposition is recorded in each of their constituent volumes.

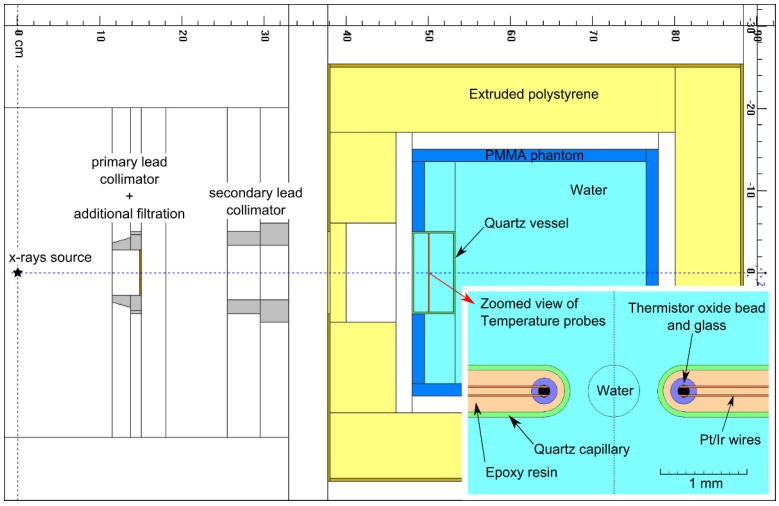

Figure 6. Horizontal section of the geometry of the water calorimeter used for energy deposition calculation with MCNPX. A zoomed view shows the end of the temperature probes.

An example of photon fluence spectrum for the ISOH300 beam (tube potential of 300 kV) obtained in air at a distance of 18 cm from the X-ray tube, and in water at a distance of 50 cm is given in Figure 7.

The radiation lateral profiles and depth dose curves in water have been measured in a water phantom with a small cylindrical ionization chamber (PTW31010) for the different reference beams. The lateral profiles were done at a depth of 2 cm in the water phantom, and a distance of 50 cm from the X-ray source. Theses radiation profiles and depth dose curves in water were also reproduced by Monte-Carlo simulations. To take into consideration the response of the chamber with the medium energy X-rays the chamber has been included in the simulation. For this, the geometry of the quartz vessel is removed from the water phantom and replaced by the geometry of the ionization chamber (cavity, walls and central electrode). A maximal difference of 0.6% is observed between measured and simulated curves for all reference beams. An example of comparison between measurements and simulations for the ISOH300 beam is given in Figure 8. The difference between the measured and calculated lateral profile along the horizontal axis in water (on the side of the field), is due to the small differences between the real geometry of the X-ray tube, and the supplier data used in Monte-Carlo simulation. But the agreement is satisfactory enough (less than 1%) to calculate the heat deposition in water calorimeter by Monte-Carlo.

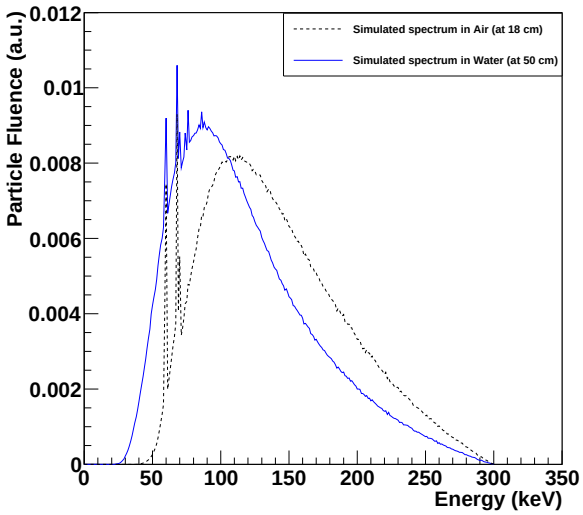

Figure 7. Simulated photon fluence spectrum in air and water, obtained on respective distances of 18 cm in air and 50 cm in water from the X-ray tube, for ISOH300 medium energy X-rays (the spectra are normalized to their integral).

3.2.2. Heat deposition and heat transfer calculation The thermal effects of the quartz vessel and the temperature probes are calculated separately with the finite-element COMSOL software [26]. Since their dimensions are two orders magnitude different it

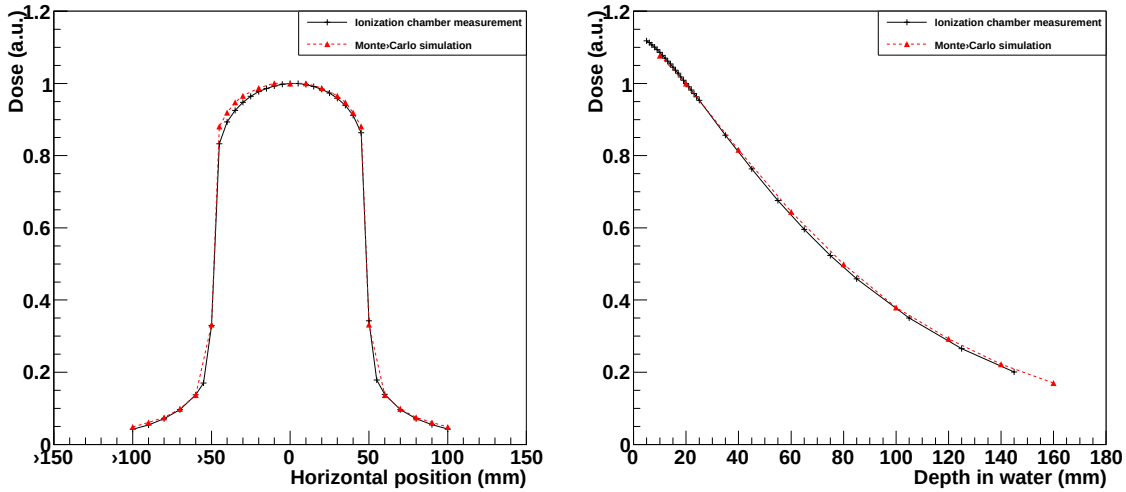

Figure 8. Absorbed dose in water lateral profile along the horizontal axis, at 2 cm depth (left), and central axis depth dose (right) for ISOH300 medium-energy X-ray beam. The type A uncertainties for ionization chamber measurements and Monte-Carlo simulations are smaller than the size of the markers in the figures.

is difficult to match the mesh elements at the boundary of the quartz probe with the mesh elements in the water inside the quartz vessel.

The geometry used in the finite-element code for calculating the effect of the quartz vessel is exactly matching the one used in the MCNPX Monte-Carlo code for energy deposition calculation, e.g. the quartz vessel inserted in front of the PMMA phantom filled with water. In MCNPX, the energy deposition by all particle sources and by unit of volume, in the water phantom and the quartz vessel, is recorded in each voxel of a rectangular and cylindrical mesh grid. A text file is filled with these values interpolated on a rectangular grid that can be used by the COMSOL code. In this code, this file is used as a heat source (function of space coordinates) for thermal transfer calculations. The temperature curve is given by the temperature drift with time inside the quartz vessel at a depth of 2 cm in water.

To calculate the effect of temperature probes with the COMSOL code, the geometry used includes the last centimeter of the end of a probe and a small volume ($1 \times 2 \times 2$ cm^3) of water around it. The mesh grids of MCNPX are not used here for recording the energy deposition in temperature probes, because the size of the voxels needed would be too small to cover the geometry of thermistor bead or quartz capillary. Instead the averaged energy deposition in each volume, at the end of modeled thermistor probe, is recorded separately. These volumes comprise the glass-coated bead thermistor, the Pt/Ir wires of the thermistor, the epoxy resin inside the capillary, the walls of quartz capillary and water in a few millimeters at the end of temperature probe (see Figure 6). These values of energy deposition in each volume of the temperature probe obtained from MCNPX code, are used as heat sources in COMSOL calculations. The geometry of the

probe in COMSOL is the same as the one used in Monte-Carlo simulation. To get the contribution of the second temperature probe, a mirror symmetry boundary condition is used on a face of the cubic water volume centered on the end of the thermistor. On the other faces the boundaries conditions are set as thermal insulation. The temperature curve is given by the evolution of temperature with time in the center of the oxide bead of the thermistor.

The temperature curves of the quartz vessel and temperature probe are combined together, and the temperature rise $(\Delta T)_{quartz\ vessel\ \&\ probes}$ for each of the 3 irradiation steps are calculated and compared to the temperature rise $(\Delta T)_{water}$ obtained from the temperature reference curve. The temperature rise is calculated using the same method as experimentally (extrapolation of linear fits to mid-irradiation) with the same parameters (delay of 80 s for post-irradiation measurements). For the quartz vessel, the reference temperature curve is obtained by a simulation with a the thermal conduction of materials equal to zero, and for temperature probes by a calculation with quartz material replaced by water. The thermal conduction correction factor (k_c) is the ratio between the calculated temperature rise $(\Delta T)_{quartz\ vessel\ \&\ probes}$ and $(\Delta T)_{water}$ for each of the 3 consecutive irradiation steps. An example of simulated temperature curves for the ISOH300 x-rays beam is given in Figure 9.

The effect of the temperature probes is visible as a peak which occurs after irradiation stop. The intensity of the peak is more important for low-energy X-ray beams. The intensity of the peak decreases fast (after 10 to 20 s), but a local minimum can be seen on the temperature curve around 40 to 60 s after the irradiation stop. It corresponds to the transition between the tail of the temperature peak after the irradiation stop (due to the thermal effect of probe vanishing), and the increasing thermal effect of the quartz vessel. To minimize the effect of temperature probes on the thermal conduction correction factor and the measured temperature rise, it was chosen to do post-irradiation linear fits with the values obtained later than 80 s after the irradiation stop. Moreover, the exact geometry and material composition of temperature probes is not well known.

The uncertainty on the thermal conduction correction factor is the quadratic sum of two terms. The first one includes the uncertainty on the thermal conduction calculation from the Monte-Carlo simulation of energy deposition, and the uncertainty coming from the geometry and material parameters of the quartz vessel. It is estimated around 0.1%. The second one takes into account the remaining effect of the temperature probe on the calculation of the temperature rise ΔT. It is estimated as the relative difference of thermal conduction correction factors calculated with a delay of respectively 80 s and 40 s for post-irradiation measurements. This difference ranges from $\sim 0.08\%$ for the ISOH300 beam to $\sim 0.4\%$ for the RQR6 beam.

In the Table 2 are given the calculated values of k_c for the 6 X-ray beams used, for each of the 3 consecutive irradiations of a sequence, with their estimated relative uncertainty ($k = 1$). Each single experimental irradiation is corrected individually taking account of its position (first, second or third) in the sequence of irradiations.

The correction factor can reach 4% for the low-energy RQR6 beam (tube potential of 80 kV).

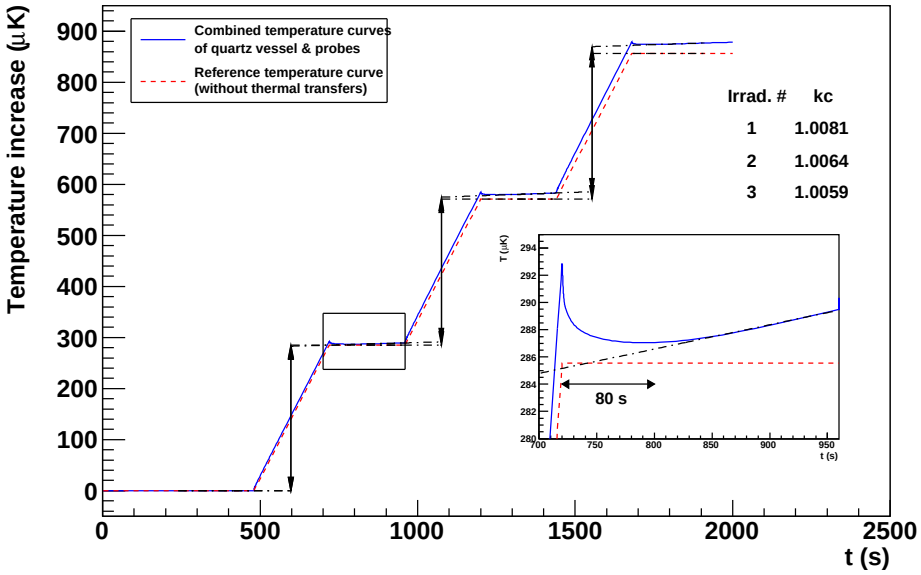

Figure 9. Thermal conduction correction factor for the ISOH300 beam calculated from the combined temperature curves of quartz vessel and probes, for a sequence of 3 irradiations of 4 minutes. In the zoomed figure one can see the peak which occurs after the irradiation stop, and which is the effect of the temperature probes.

3.3. Radiation field perturbation correction factor (k_p)

The radiation field is perturbed by the calorimeter non-water materials. The perturbation comes first from the thermal enclosure, and particularly from the insulating materials inside the calorimeter window. The second perturbation is due to the quartz vessel and the temperature probes. The third perturbation comes from design differences between the water phantom of the calorimeter and the reference water phantom used for ionization chamber calibration (position and diameter of their quartz window).

The perturbation factor due to the thermal enclosure is determined both by ionization chamber measurements and Monte-Carlo simulations. An ionization chamber is placed at the same depth in water (2 cm) as the temperature probes inside the special water phantom used for ionization chamber calibration. This special phantom also presents a 0.8 mm thick quartz window (of ∅12 cm), so that the only difference with the calorimeter phantom lies in the lateral and back walls of the quartz vessel.

The radiation field perturbation factor due to the thermal enclosure is then measured as the ratio between the current given by the ionization chamber measured with and without the front part of the thermal enclosure (Table 3). The ratio ranges from 1.012 to 1.051 depending on the X-ray beam. Monte-Carlo simulations were done

Table 2. Thermal conduction correction factor (k_c). The relative uncertainties are given at $k = 1$.

X ray beam ref.	k_c	u(%)
RQR6	1.0406	
	1.0295	0.44
	1.0302	
RQR9	1.0276	
	1.0197	0.43
	1.0198	
RQR10	1.0232	
	1.0161	0.38
	1.0160	
CCRI180	1.0144	
	1.0107	0.24
	1.0099	
CCRI250	1.0081	
	1.0062	0.14
	1.0056	
ISOH300	1.0081	
	1.0064	0.13
	1.0059	

to check this value. There was a good agreement with the measurements for medium-energy X-ray beams around 250 and 300 kV, but discrepancies at lower energies are observed (Figure 10). Now, the commercial polystyrene contains a proportion of 0.8 to 4% in mass of bromine [27] due to the addition of fire retardants. To verify this, we performed a low-energy X-ray spectroscopy of a polystyrene sample used in our calorimeter (Figure 11). The spectrum showed characteristic peaks of fluorescence $K_{\alpha 1}$ and $K_{\beta 1}$ of bromine. The measurement results can be well reproduced with Monte-Carlo simulations by adding a proportion of 2.5% in mass of bromine in polystyrene.

Monte-Carlo simulations were also used to calculate the perturbation of the radiation field by the quartz vessel (Table 3). The results for the factor ranges from 1.002 to 1.013 following the energy of X-ray beams. The effect of temperature probes is much smaller than the one of quartz vessel and was neglected (the measurement, or simulation of this effect is particularly difficult because of the small size of the probes). The simulation also takes into account the perturbation coming from small design differences between the water phantoms used for calorimetry and for ionization chamber measurements (position and diameter of their front quartz window).

The uncertainties on the radiation field perturbation factor due to the calorimeter thermal enclosure, are the type A uncertainties on the ratio of currents measured by ionization chamber. For the radiation field perturbation factor due to the quartz vessel

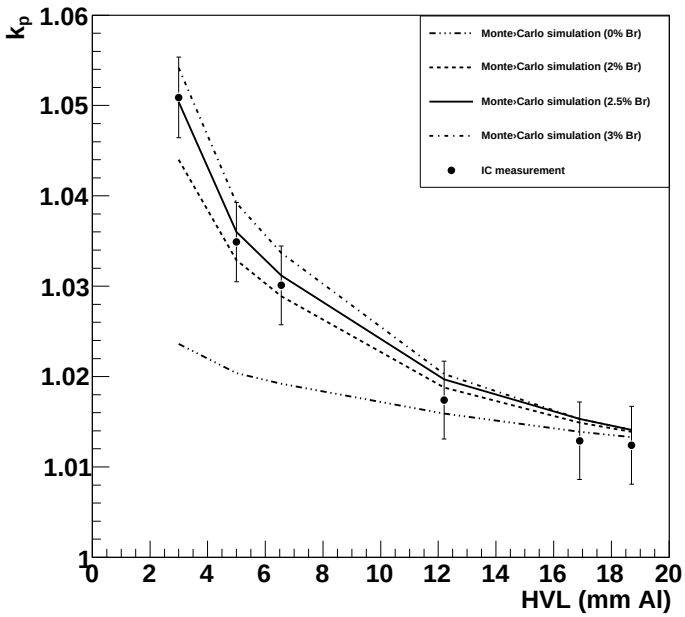

Figure 10. Thermal enclosure dosimetric perturbation factor (k_p) as function of X-ray HVL (in equivalent Al thickness). The ionization chamber measurement results (black dots) for the 6 X-ray reference beams overlap the results of Monte-Carlo simulations (lines) obtained with an increased percentage in mass of bromine in polystyrene composition.

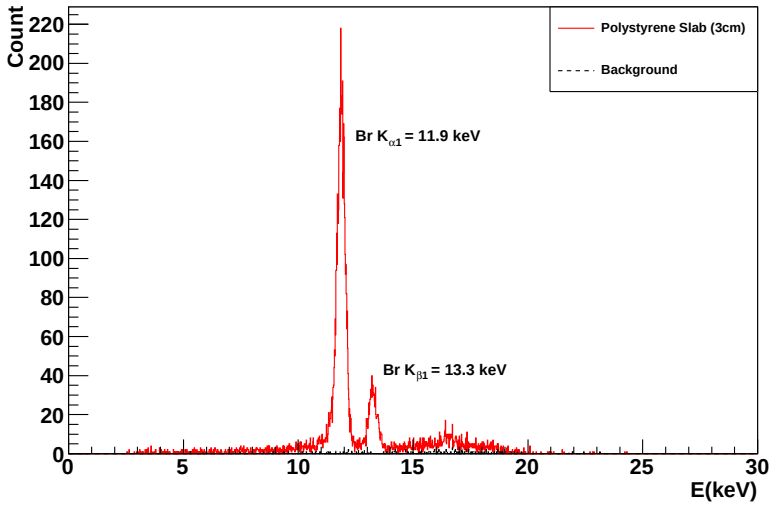

Figure 11. Low energy X-ray spectrum of polystyrene sample used in calorimeter window.

and the water phantom, the uncertainties are the type A uncertainties given by the Monte-Carlo code.

Table 3. Radiation field perturbation factor (k_p) due to the calorimeter thermal enclosure, quartz vessel and water phantom. The relative uncertainties are given at $k = 1$.

X ray beam ref.	k_{p1} (thermal enclosure)		k_{p2} (quartz vessel and water phantom)		$k_p = k_{p1} \cdot k_{p2}$	
		u(%)		u(%)		u(%)
RQR6	1.0509	0.17	1.0126	0.11	1.0641	0.21
RQR9	1.0349	0.16	1.0122	0.11	1.0475	0.20
RQR10	1.0301	0.14	1.0107	0.11	1.0411	0.18
CCRI180	1.0174	0.14	1.0081	0.11	1.0257	0.18
CCRI250	1.0129	0.13	1.0031	0.11	1.0161	0.17
ISOH300	1.0124	0.24	1.0022	0.11	1.0146	0.26

3.4. Water chemical heat defect (h)

All the energy deposited by radiation in water is not converted into heat, this effect is named heat defect of water h. The heat defect of water depends on the content of gases dissolved in water, impurities and the type of radiation. For high-purity water saturated with an inert gas like nitrogen or argon, in the absence of a gas-volume, a stationary state is reached after a small accumulated dose, and the heat defect measured and predicted by radiolysis models is zero [28, 29, 30]. If a gas-volume is in contact with water, then there is an accumulation inside the gas-volume of the volatile compounds such as O_2 and H_2 that are either initially present in water, or produced in water by radiolysis. And the continuous transfer of these gases between the gas-volume and the water changes the heat defect. In our case, the quartz vessel is filled with high-purity water saturated with N_2 gas, and a pre-irradiation of the water vessel at several hundred grays is done to stabilize the heat defect before measurements. In high-energy photon or electron beams, for which the linear-energy-transfer (LET) is low (0.2 keV/μm), the heat defect of ultra-pure water saturated with N_2 gas is zero. In medium-energy X-ray beams, the LET is between 2 keV/μm and 6 keV/μm for a X-ray energy of 200 keV and 50 keV [31] respectively. Simulations of the water radiolysis were done for such a LET and the value of the heat defect is found endothermic ($h > 0$) and between 0.02% and 0.1% (for ultra-pure water perfectly saturated with N_2 gas, and without any impurities). Similar calculations based on real measurements of the dissolved oxygen concentration and organic carbon impurities allowed also to estimate the uncertainty on the heat defect of water. The value obtained is about 0.3% and is in agreement with those used by other metrology laboratories [32, 33, 34, 35, 36]. So the heat defect of water for medium-energy X-rays was taken as zero with a 0.3% relative standard uncertainty.

3.5. Density of water correction factor (k_ρ)

The density of water changes between 4 °C (temperature of calorimetric measurements) and 20 °C (reference temperature for ionometric measurements). So the measured absorbed dose to water must be corrected for this effect. For this the dose gradient at the depth of 2 cm in water for the different reference beams must be known. It is obtained from the central axis depth dose profile in water calculated with MCNPX. This correction factor ranges from 1.00018 (for ISOH300) to 1.00060 (for RQR6), with a relative uncertainty of 0.038% to 0.011%.

3.6. Depth-in-water correction factor (k_d)

The depth in water of temperature probes is measured by the optical system already described and can be slightly different from the target value of 2 cm. Then the measured absorbed dose to water is corrected (k_d depth-in-water correction factor) for this depth difference by using the value of the dose gradient obtained from Monte-Carlo simulation. This correction factor ranges from 1.0007 (for ISOH300) to 1.0023 (for RQR6), with a relative uncertainty of 0.15% and 0.04%.

4. Absorbed dose to water measured by water calorimetry in medium-energy X-ray beams

The absorbed dose rate to water was measured for the 6 medium-energy X-ray beams. The average number of measurements done for each of the 6 beams is about one hundred. The statistical uncertainty on the temperature rise ranges from 0.24% to 0.40% (table 5). To obtain the value of the absorbed dose, equation 2 was applied with the correction factor values detailed in the previous section. An example of uncertainty budget for the ISOH300 X-ray beam is given in table 4. The final combined relative standard uncertainty for the 6 beams ranges from 0.49% (for CCRI250) to 0.72% (for RQR6) (table 5). It is worth noting that the two predominant uncertainty components (except ΔT measurement reproducibility) are those related to the heat defect of water and the radiation field perturbation correction factor.

5. Conclusion

A new water calorimeter has been designed and optimized at LNE-LNHB for primary measurements of absorbed dose at low depth in water (down to 0.5 cm). This makes possible to establish primary references for medium-energy X-ray in agreement with dosimetry protocol recommendations. Such measurements for 6 medium energy X-ray reference beams (from 80 kV to 300 kV) have been done at a depth of 2 cm in water. The correction factors to be applied have been determined for each of the reference beams. The absorbed dose to water obtained has a combined relative standard uncertainty between 0.49% and 0.72% following the X-ray beam quality.

Table 4. Uncertainty budget for the absorbed dose rate to water $\dot{D}_W$ measurement in the ISOH300 x-ray beam.

Source of uncertainty	Value	Relative uncertainty (%) s_i	u_j
Specific heat capacity of water ($J.kg^{-1}.K^{-1}$)	4204.8	–	0.1
ΔT measurement reproducibility (N=102)	–	0.28	–
Temperature probe positioning	–	–	0.06
Heat defect of water h	0.0	–	0.3
Thermal conduction correction factor k_c	[a]	–	0.13
Radiation field perturbation correction factor k_p	1.0146	–	0.26
Density of water correction factor k_ρ	1.00018	–	0.038
Temperature probe depth-in-water correction factor k_d	1.0007	–	0.15
Temperature probe calibration	–	–	0.1
Irradiation time	–	0.027	–
Quadratic summation		0.28	0.47
Combined relative standard uncertainty (u_c) on $\dot{D}_W$ ($k = 1$)			0.55

[a] Thermal conduction correction factor ($t_{irr.} = 240$ s) applied to each of the three consecutive irradiations of 4 min of one acquisition sequence : $k_c = 1.0081, 1.0064, 1.0059$

Table 5. Absorbed dose rate to water measured in medium energy X-ray beams.

X-ray beam ref.	Number of meas.	ΔT (μK) Value	s(%)	$\dot{D}_W$ ($Gy.min^{-1}$) Value	u_c(%)
RQR6	102	282.60	0.40	0.3292	0.72
RQR9	114	314.58	0.39	0.3559	0.71
RQR10	96	477.38	0.23	0.5336	0.64
CCRI180	108	386.84	0.29	0.4244	0.56
CCRI250	72	495.52	0.24	0.5358	0.49
ISOH300	102	375.52	0.28	0.4055	0.55

Acknowledgments

We wish to thank B. Chauvenet and Arul Selvi for their useful comments on the manuscript.

References

[1] IAEA Technical Reports Series No. 277. *Absorbed Dose Determination in Photon and Electron Beams*. 1997.

[2] C.-M. Ma (Chair), C. W. Coffey, L. A. DeWerd, C. Liu, R. Nath, S. M. Seltzer, and J. P. Seuntjens. AAPM protocol for 40–300 kV X-ray beam dosimetry in radiotherapy and radiobiology. *Medical Physics*, 28(6):868–893, 2001.

[3] S. C. Klevenhagen (Chair), R. J. Aukett, R. M. Harrison, C. Moretti, A. E. Nahum, and K. E. Rosser. The IPEMB code of practice for the determination of absorbed dose for x-rays below

300 kV generating potential (0.035 mm Al - 4 mm Cu HVL; 10 - 300 kV generating potential). *Physics in Medicine and Biology*, 41(12):2605, 1996.

[4] T. W. M. Grimbergen, A. H. L. Aalbers, B. J. Mijnheer, J. Seuntjens, H. Thierens, J. Van Dam, F. W. Wittkämper, and J. Zoetelief. Dosimetry of low and medium energy x-rays - a code of practice for use in radiotherapy and radiobiology. *NCS Report 10*, 1997.

[5] IAEA Technical Reports Series No. 398. *Absorbed Dose Determination in External Beam Radiotherapy*. 2000.

[6] J. Seuntjens. *Comparative study of ion chamber dosimetry and water calorimetry in medium energy X-ray beams*. PhD thesis, Rijksuniversiteit Gent, 1991.

[7] L. A. de Prez and J. A. de Pooter. The new NMi orthovolt X-rays absorbed dose to water primary standard based on water calorimetry. *Phys. Med. Biol.* , **53**(13):3531–3542, 2008.

[8] A. Krauss. Application of water calorimetry as absorbed dose to water standards for radiotherapy dosimetry. In *Absorbed Dose and Air Kerma Primary Standards Workshop*, Paris, 9–11 May 2007. Absorbed Dose and Air Kerma Primary Standards Workshop, LNE, CEA-LIST-LNHB & BIPM.

[9] A Krauss, L Büermann, H-M Kramer, and H-J Selbach. Calorimetric determination of the absorbed dose to water for medium-energy X-rays with generating voltages from 70 to 280kV. *Physics in Medicine and Biology*, 57(19):6245, 2012.

[10] N. Perichon, B. Rapp, M. Denoziere, J. Daures, A. Ostrowsky, and J-M. Bordy. Comparison between absorbed dose to water standards established by water calorimetry at LNE-LNHB and by application of international air-kerma based protocols for kilovoltage medium energy X-rays. *To be publish in Physics in Medicine and Biology*.

[11] N. Perichon. *Etablissement des références nationales, en termes de dose absorbée, par calorimétrie dans l'eau, pour les faisceaux de rayons X de moyenne énergie applicables en radiothérapie.* PhD thesis, Université Paris-Sud, 2012.

[12] D T Burns, C Kessler, M Denoziere, and W Ksouri. Key comparison BIPM.RI(I)-K3 of the air-kerma standards of the LNE-LNHB, France and the BIPM in medium-energy X-rays. *Metrologia*, 45(1A):06004, 2008.

[13] GE Measurement & Control. Radiography (X-ray) (formerly SEIFERT NDT). `http://www.ge-mcs.com/en/radiography-x-ray.html`.

[14] COMET. X-ray sources. `http://www.comet-xray.com/`.

[15] C. K. Ross and N. V. Klassen. Water calorimetry for radiation dosimetry. *Phys. Med. Biol.* , **41**(1):1–29, 1996.

[16] B. Rapp. Development of a water calorimeter for dosimetry at LNE-LNHB. *Revue française de métrologie*, **24**(2010-4):3–8, 2010.

[17] B. Rapp. The LNE-LNHB water calorimeter: measurements in a ^{60}Co beam. In *Standards, Applications and Quality Assurance in Medical Radiation Dosimetry (IDOS)*, volume 1, page 67, Vienna, 9–12 November 2010. IAEA, 2011 Proceedings series STI/PUB/1514.

[18] VORTEC. Vortex tubes. `http://www.vortec.com`.

[19] M. R. McEwen and A. R. DuSautoy. Primary standards of absorbed dose for electron beams. *Metrologia*, 46(2):S59, 2009.

[20] K. J. Stewart. *The development of new devices for accurate radiation dose measurement: a guarded liquid ionization chamber and an electron sealed water calorimeter*. PhD thesis, McGill University, Montreal, 2007.

[21] GE Measurement & Control. Sensors & measurement. `http://www.ge-mcs.com/en/temperature/ntc-thermistors.html`.

[22] GoodFellow. `http://www.goodfellow.com`.

[23] M Zabransky, V Ruzicka Jr, V Majer, and E S Domalski. Heat Capacity of Liquids: Volume I Critical Review and Recommended Values. *J. Phys. Chem. Ref. Data*, Vol. 1(Monograph No. 6), 1996.

[24] N S Osborne, H F Stimson, and D C Ginnings. Measurements of Heat Capacity and Heat of

Vaporization of Water in the Range 0 to 100 ^{o}C. *J. Res. Natl. Bur. Stand.*, 23:197–260, 1939.

[25] MCNPX. MCNPX-Monte Carlo N-Particle Transport Code System for Multiparticle and High Energy Applications. `http://mcnpx.lanl.gov/`.

[26] COMSOL. COMSOL 3.4 Multiphysics. `http://www.comsol.com/`.

[27] M. Alaee, P. Arias, A. Sjödin, and Å. Bergman. An overview of commercially used brominated flame retardants, their applications, their use patterns in different countries/regions and possible modes of release. *Environment International*, 29(6):683–689, 2003.

[28] Norman V. Klassen and Carl K. Ross. Absorbed dose calorimetry using various aqueous solutions. *International Journal of Radiation Applications and Instrumentation. Part C. Radiation Physics and Chemistry*, 38(1):95 – 104, 1991.

[29] C. K. Ross, N. V. Klassen, and G. D. Smith. The effect of various dissolved gases on the heat defect of water. *Medical Physics*, 11(5):653–658, 1984.

[30] Achim Krauss. The PTB water calorimeter for the absolute determination of absorbed dose to water in ^{60}Co radiation. *Metrologia*, 43(3):259, 2006.

[31] ICRU report 16. *Linear Energy Transfer*. 1970.

[32] C K Ross, J Seuntjens, N V Klassen, and K R Shortt. The NRC sealed water calorimeter: correction factors and performance. In *Proc. Workshop on Recent Advances in Calorimetric Absorbed Dose Standards*, pages 90–102, National Physical Laboratory, Teddington, UK, 1999. A J Williams and K E Rosser *Rep. CIRM 42*.

[33] J. Seuntjens and S. Duane. Photon absorbed dose standards. *Metrologia*, 46(2):S39, 2009.

[34] N V Klassen and C K Ross. Water calorimetry: the heat defect. *J. Res. Natl Inst. Stand. Technol.*, 102:63–71, 1997.

[35] N V Klassen and C K Ross. Water calorimetry: a correction to the heat defect calculations. *J. Res. Natl Inst. Stand. Technol.*, 107:171–8, 2002.

[36] J Medin, C K Ross, G Stucki, N V Klassen, and J P Seuntjens. Commissioning of an NRC-type sealed water calorimeter at METAS using ^{60}Co γ-rays. *Physics in Medicine and Biology*, 49(17):4073, 2004.